Open access • Journal Article • DOI:10.1364/OL.44.002310

High extinction ratio on-chip pump-rejection filter based on cascaded grating-assisted contra-directional couplers in silicon nitride rib waveguides. — Source link

Xiaomin Nie, Nina Turk, Yang Li, Zuyang Liu ...+1 more authors

Institutions: Ghent University

Published on: 01 May 2019 - Optics Letters (Optical Society of America)

Topics: Extinction ratio, Passband, Bandwidth (signal processing), Power dividers and directional couplers and Distributed Bragg reflector

High rejection ratio on-chip pump rejection filter based on cascaded grating-assisted contra-directional couplers in silicon nitride rib waveguides

XIAOMIN NIE[1,2], YANG LI[1,2], NINA TRUK[1,2], ZUYANG LIU[1,2], AND ROEL BAETS[1,2,*]

[1] Photonics Research Group, INTEC, Ghent University-IMEC, Technologiepark 126, B-9052 Ghent, Belgium
[2] Center for Nano- and Biophotonics, Ghent University, Technologiepark 126, B-9052 Ghent, Belgium
[*] Corresponding author: Roel.Baets@UGent.be

Compiled March 7, 2019

We present an on-chip filter that is based on the grating-assisted contra-directional coupler (GACDC) implemented on a silicon nitride rib waveguide platform. This filter enjoys the benefit of an unlimited free spectral range (FSR) on the red side of the stop/pass band. Not like a Bragg reflector, the GACDC filter has the advantage of coupling the rejected light into a bus waveguide, instead of reflecting it into the input. This property makes it an add/drop filter suitable for pump rejection and allows effective cascading between multiple stages to provide even higher rejection ratio compared to the single stage version. In this work, we experimentally show that a 16-stage cascaded GACDC filter possesses a stop band with a bandwidth smaller than 3 nm and rejection ratio as high as 68.5 dB.

http://dx.doi.org/10.1364/ao.XX.XXXXXX

Recently, silicon nitride (SiN) has become one of the most prominent platforms for the miniaturization of photonic circuits in the visible or near infrared range (< 1 μm), where the silicon is no longer transparent [1]. Like the silicon-on-insulator (SOI) technology, SiN nanophotonics is also a CMOS-compatible technology that allows large-scale, cost-effective fabrication of photonic integrated circuits together with the possibility to co-integrate the electronics.

A wide range of high-performance components, including grating couplers [2], polarization splitters [3], and wavelength selective filters [4], have been developed on the silicon nitride platform to open the road to further integration of complicated on-chip systems[5–7]. As an essential component, the on-chip wavelength filter has attracted a lot of attention from researchers interested in on-chip lasers [8], optical sensors [9] as well as wavelength-division multiplexers [10]. Filters based on the Bragg gratings, ring resonators, and Mach-Zehnder cascades have been studied and demonstrated to meet the requirement of various applications [9–11]. Compared to the ring-resonator filters, grating based filters such as Bragg reflectors have an unlimited free spectral range (FSR). This is important to applications such as on-chip Raman spectroscopic systems [12], which require filters with a high rejection ratio at the pump wavelength and a flat spectral response in the wavelength range where the Raman signals are generated. Bragg reflectors can fulfill these requirements. However, to prevent the reflected light from going back to the integrated laser, one would also need to integrate an on-chip circulator [13], which adds extra complexity and cost to the system. A filter based on the grating assisted contra-directional coupler (GACDC) provides a better solution. While having a flat spectral response aside from the stop band, the GACDC filter also allows coupling of the rejected light contra-directionally into a bus waveguide. Due to this property, GACDC filters are not only suitable for pump rejection but also attractive to the researchers interested in wavelength-division multiplexing. As add/drop filters, GACDC filters were firstly implemented on the planar optical waveguides platform with silica and III-V materials [14], followed by the more recent implementations on the SOI platform [15–17].

In this Letter, we implement the GACDC filters on the SiN platform. Aiming at the applications such as the pump-rejection filters for bio-sensing spectroscopic systems operating in the near infrared region, we target the center wavelength of the stop band at the often used 785 nm. This would require gratings with the period smaller than what is allowed by the conventional 193 nm deep-UV lithography [18]. In this case, e-beam lithography is used for prototyping the proposed devices which, in the future, can also be realized by the deep-UV immersion lithography in a CMOS fab [19].

The proposed filters are based on the GACDC, which consists of a narrow rib waveguide (waveguide *a*), a wide rib waveguide (waveguide *b*), and a grating between the two waveguides. As shown in figure 1 (a), a single stage GACDC filter uses grating couplers as I/O ports and has waveguide tapers to connect them to the GACDC. By connecting multiple GACDCs, one can easily construct a cascaded GACDC filter, such as the 4-stage cascaded GACDC filter shown in figure 1 (b). Measured from the scanning electron microscopy (SEM) image of the coupler region shown in figure 1 (c), the fabricated devices have a width of waveguide *a*,

W_a = 330 nm, a width of waveguide b, W_b = 585 nm. The grating has a width W_g = 320 nm, a period Λ = 244 nm and a duty cycle around 50%. To obtain a proper coupling strength κ, we set the spacing between the two waveguides to 750 nm and shift the grating for 80 nm from the center to waveguide b. In the mode-transition regions on the two sides of each coupler, we designed bending tapers to bring the two waveguides close to each other as well as to separate them from each other. Figure 1 (d) shows the SEM image where waveguide b is approaching waveguide a and figure 1 (e) pictures the mode-transition regions of the cascaded GACDC filter.

The working principle is also illustrated in figure 1 (c). While the co-directional coupling is suppressed since the fundamental TE-like modes in waveguide a and b have different propagating constants determined by their wavelength-dependent effective indices (n_a and n_b), the contra-directional coupling can happen with the assistance of the grating. Light with wavelength $\lambda_a = 2n_a\Lambda$ can be reflected back to the input port due to the intra-waveguide Bragg reflection while the inter-waveguide contra-directional coupling can reflect the light with wavelength $\lambda_D = (n_a + n_b)\Lambda$ to the drop port. As a result, the transmission spectrum measured at the through port will possess two stop bands corresponding to the intra-waveguide Bragg reflection and the inter-waveguide reflection induced by the contra-directional coupling. For the convenience of the discussion, we refer the two stop bands as self-reflection band and cross-reflection band respectively.

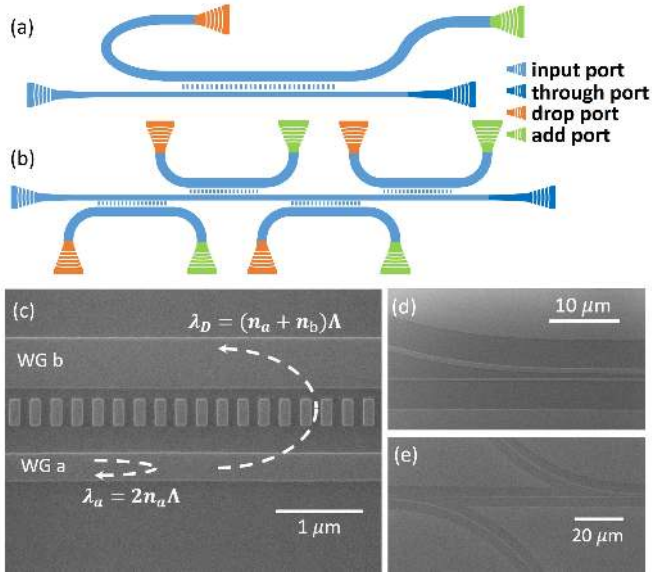

Fig. 1. Sketches of (a) the single stage CDC filter and (b) the 4-stage cascaded CDC filter. SEM pictures of (c) the coupler region with illustrations of the intra-waveguide Bragg reflection and the inter-waveguide reflection induced by the contra-directional coupling; (d) the mode-transition region where waveguide b is approaching waveguide a; (e) the mode-transition region in the cascaded GACDC filter.

We solve the fundamental TE-like modes in the coupler region with the mode solver FIMMWAVE. Figure 2(a) shows the cross-section with the calculated intensity profiles of the fundamental TE-like modes in both rib waveguides. In the simulation, we set both the rib height and slab thickness to 150 nm. In figure 2(b), we plot the effective indices of the modes in waveguide a and b as the function of the wavelength. By adding the average of the indices and the curve $y = \lambda/(2\Lambda)$, we can find λ_D around 785 nm and λ_a around 774 nm.

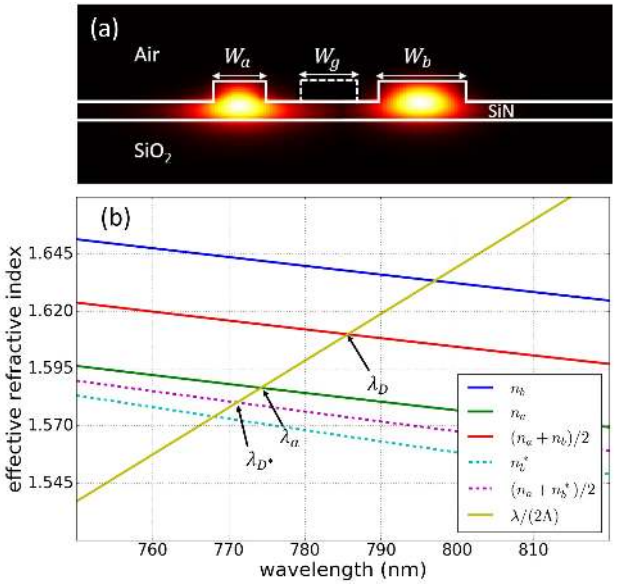

Fig. 2. (a) the cross section of the coupler region with the calculated intensity profiles of the fundamental TE-like modes of both rib waveguides; (b) the dispersion curves of the modes with phase matching wavelengths indicated with arrows and labels.

Apart from the position of the stop bands, we are also interested in the rejection ratio that can be achieved by the device. According to the mode coupling theory [20], for a grating based reflector with total grating length L, the peak reflection at the center wavelength of the stop band can be written as

$$R = \tanh^2 |\kappa|^2 L \quad \textbf{(1)}$$

This means, theoretically, an arbitrary high rejection ratio can be obtained by increasing the total length of the grating. Realistically, however, the rejection ratio will saturate around 40 dB beyond a certain filter length [11, 21, 22]. Such saturation is believed to originate from the phase errors induced by fabrication imperfections. To understand this, we first think of a Bragg reflector without any fabrication imperfection. In this ideal reflector, the injected light propagating in the forward direction is continuously reflected by the grating units into the backward-propagating mode. At the Bragg wavelength, the periodicity of the grating units ensures that all partial reflections are in phase and interfere constructively. Although the reflected light propagating in the backward direction needs to travel through the grating and is therefore subject to secondary grating diffraction, the resulting contributions to the forward-propagating light will actually be out of phase with the original light coming from the input, thereby helping the input light to decay exponentially. However, in real life, even a very small fabrication imperfection can cause a phase error and create deviations in the phase relationships of all contributing field components. Such a phase error will therefore scatter the reflected light and allow a tiny amount of light to travel towards the through port. And, as the length of the grating increases, more and more contributions (with phase errors) will play a role and accumulate to set a certain saturation level and limit the achievable rejection ratio.

To surpass this limitation and achieve higher rejection ratio, an effective way, as introduced in [23], is to remove the reflected light before it can propagate through many grating units. We can easily implement this strategy with the cascaded GACDC filters. In a cascaded GACDC filter such as the example shown in figure 1(b), the light coupled contra-directionally to the bus waveguides can be coupled out through the drop ports before they can travel too far.

To characterize the fabricated devices, we use a setup containing two cleaved single mode fibers (780HP) that are positioned near-vertically (10 degrees away from normal) to the chip. Light is coupled into and out of the chip through the on-chip grating couplers. To obtain the transmission spectra with sub-nanometer resolution (0.3 nm) in the wavelength range that is interesting for us, we use a Ti: Sapphire tunable CW laser (SOLSTIS, M2) as the light source and an optical power meter (HP 8153A) to measure the transmitted power.

We first measured the transmission spectra for the single stage GACDC filters that have different filter length, L= 150, 300, 600, 1000, 2000 and 3000 μm. In the spectra shown in figure 3 (a), two notches centered around 772.0 nm and 783.6 nm can be observed corresponding to the self-reflection and cross-reflection band. A third dip centered at 769.2 nm could be explained by the contra-directional coupling between the forward-propagating mode in waveguide a and a high order TM-like backward-propagating mode in waveguide b. This three wavelengths are in agreement with the three intersections labeled with λ_a, λ_D and λ_{D^*} in figure 1 (e). The small discrepancy could be explained by the uncertainties in the etch depth.

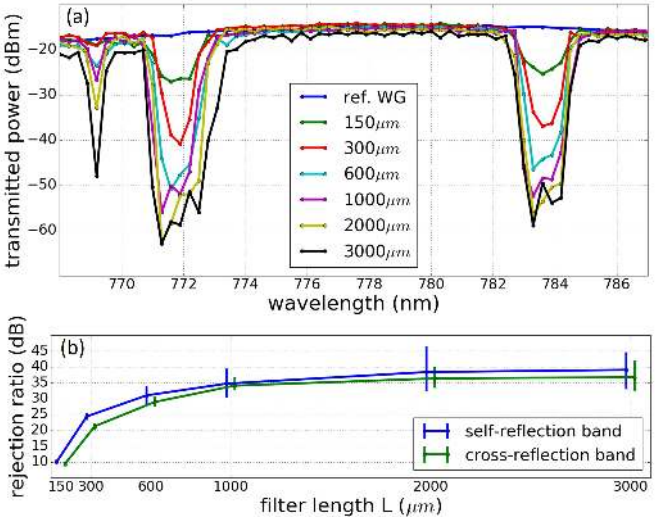

Fig. 3. (a) Measured transmission spectra of a reference rib waveguide and GACDC filters with filter length L = 150, 300, 600, 1000, 2000 and 3000 μm; (b) the calculated average rejection ratio in both stop bands plotted as function of filter length L. In (b) the two curves are shifted for better visualization.

To better observe the trend of the saturation, we need to estimate the average rejection ratio as the spectral response of inside the stop bands are not smooth, especially for the devices that have large filter length. The approach is to average the transmitted power measured around the center wavelengths of the stop bands and normalize it to the averaged transmitted power measured outside the stop bands. In Figure 2(b), we plot the average rejection ratio of both stop bands as a function of the filter length L, with the error bars indicate the maximum and minimum rejection ratio inside the stop bands. From the curves, we can see that while the average rejection ratio of the cross-reflection band is lower than of the self-reflection band, they both increase with the filter length. As expected, the increment decreases for large filter length. And beyond 2000 μm, the rejection ratio almost stops increasing and saturates to around 40 dB.

To show that the cascaded GACDC filters have higher rejection ratio, we consider a set of cascaded GACDC filters that have the same total filter length (2000 μm) and the different number of stages. We measure the transmission spectra for the cascaded GACDC filters that have 4, 8, 10 and 16 stages and show the spectra in figure 4(a) together with the spectrum measured from a single stage GACDC filter that has filter length L = 2000 μm and a reference waveguide. From the spectra, we calculate the average rejection ratio in both stop bands and plot them in figure 4(b) as the function of the number of stages.

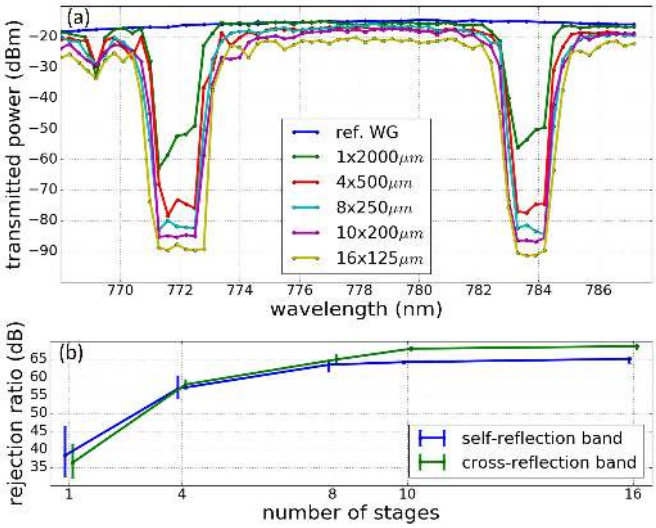

Fig. 4. (a) Measured transmission spectra of a reference rib waveguide, a single stage GACDC filter with filter length L = 2000 μm and cascade GACDC filters that have the same total length (2000 μm) and different number of stages (4, 8, 10 and 16); (b) the calculated average rejection ratio in both stop bands plotted as function of the number of stages. In (b) the two curves are shifted for better visualization.

Immediately, we can see that the cascaded GACDC filters provide higher rejection ratio compared to the single stage filter that has the same filter length in the cross-reflection band. This is because that, although the phase errors introduced by the fabrication imperfections are still there, most of the reflections are coupled out from the drop ports before they can interact with the grating units in previous stages. As the number of stages increases, the reflections are removed more frequently, allowing the filter to suffer less from the phase errors and therefore have a higher rejection ratio. However, although we managed to remove most of the reflections, still a small portion can survive and be coupled into waveguide a. This small portion of reflections, propagating in waveguide a, are subject to the secondary grating diffraction, and therefore contribute to the forward-propagating light that can reach the through port and set a new limitation to the achievable rejection ratio.

The spectra shown in 4 (a) and the trend plotted in 4 (b)

are in line with our expectations. From the 16-stage cascaded GACDC filter, we measured the highest average rejection ratio up to 68.5 dB in the cross-reflection band that has a bandwidth less than 3 nm. This is an improvement close to 30 dB when compared to what is achieved by the single stage GACDC filter that has the same total filter length.

Another interesting phenomenon is that the rejection ratio of the self-reflection band is also increased. Nevertheless, it is worth noticing that while the rejection ratio of the cross-reflection band is lower than that of the self-reflection band in the case of a single stage GACDC filter, now the situation is reversed. This means the rejection ratio in the self-reflection band is improved less than that in the cross-reflection band.

Two possible reasons could lead to this improvement. On the one hand, in the mode-transition regions where waveguide b is approaching to or distancing from waveguide a, only 96.6% of the power stays in waveguide a while the rest is coupled into waveguide b according to the simulation. This equals to a loss of -0.15 dB per taper if light propagates through it. Such a small loss is negligible for the single stage GACDC filter as it only has two tapers. However, for a cascaded GACDC filter with many stages, the total loss experienced by the light propagating directly from the input port to the through port becomes non-negligible. For instance, in the 16-stage cascaded GACDC filter, light travels through all 32 tapers will experience a total loss of around -4.8 dB. This also agrees with the downshifting of the measured spectra in 4 (a). For light with wavelengths inside the self-reflection band, the situation is even worse, and they will experience more loss. As an example, in the worst case, light reflected at almost the end of the grating will propagate backward in waveguide a to almost the beginning of the grating where it is partly reflected due to a phase error there, reversing its direction and propagating towards the through port. This light, though finally managed to the through port, has to travel through most of the tapers for multiple times and therefore is greatly attenuated. More generally, inside the self-reflection band, most of light has to travel through tapers for multiple times if they want to reach the through port and contribute to the saturation. Consequently, for the cascaded GACDC filters with more stages, the rejection ratio inside the self-reflection band is increased. On the other hand, in the coupler regions, as waveguide a has a small width W_a = 330 nm and is placed only 750 nm away from waveguide b, the fundamental TE-like mode in waveguide a is loosely confined and slightly pulled to waveguide b. This means, even the intra-waveguide reflection happens mostly in waveguide a, a small amount of light can also be scattered into the bus waveguide and propagates in the backward direction. With this part of light coupled out from the drop ports, we removed the possibility that they could be scattered back again into waveguide a and propagate to the through port. To some extent, this also helps increase the rejection ratio inside the self-reflection band.

To summarize, we have demonstrated the implementation of on-chip GACDC filters that have cross-reflection band in the near infrared wavelength range on a silicon nitride rib waveguide platform. Experimentally, we showed that the average rejection ratio saturates to less than 40 dB for single stage GACDC filters with filter length beyond 2000 μm. We proved that GACDC filters could be cascaded to obtain rejection ratio higher than this saturation level. The best result we measured from a 16-stage cascaded GACDC filter has a stop band centered at the inter-waveguide contra-directional coupling wavelength λ_D = 783.6 nm with a bandwidth less than 3 nm and an average rejection ratio up to 68.5 dB. In conclusion, by coupling the rejected light into the bus waveguides, the demonstrated on-chip GACDC filters can provide a stop band with a high rejection ratio and an unlimited FSR on the red side of it. These properties make the on-chip GACDC filters suitable and promising for pump rejecting in applications such as the on-chip Raman spectroscopy.

REFERENCES

1. A. Rahim, E. Ryckeboer, A. Z. Subramanian, S. Clemmen, B. Kuyken, A. Dhakal, A. Raza, A. Hermans, M. Muneeb, S. Dhoore *et al.*, J. Light. Technol. **35**, 639 (2017).
2. A. Z. Subramanian, S. Selvaraja, P. Verheyen, A. Dhakal, K. Komorowska, and R. Baets, IEEE Photonics Technol. Lett. **24**, 1700 (2012).
3. X. Sun, M. Alam, J. Aitchison, and M. Mojahedi, Opt. letters **41**, 163 (2016).
4. D. Dai, Z. Wang, J. F. Bauters, M.-C. Tien, M. J. Heck, D. J. Blumenthal, and J. E. Bowers, Opt. express **19**, 14130 (2011).
5. E. Ryckeboer, X. Nie, A. Z. Subramanian, D. Martens, P. Bienstman, S. Clemmen, S. Severi, R. Jansen, G. Roelkens, and R. Baets, **9891**, 98911K (2016).
6. Y. Zuta, I. Goykhman, B. Desiatov, and U. Levy, Opt. Express **18**, 24762 (2010).
7. S. Ramelow, A. Farsi, S. Clemmen, D. Orquiza, K. Luke, M. Lipson, and A. L. Gaeta, arXiv preprint arXiv:1508.04358 (2015).
8. W. Xie, T. Stöferle, G. Raino, T. Aubert, S. Bisschop, Y. Zhu, R. F. Mahrt, P. Geiregat, E. Brainis, Z. Hens *et al.*, Adv. Mater. **29**, 1604866 (2017).
9. K. De Vos, I. Bartolozzi, E. Schacht, P. Bienstman, and R. Baets, Opt. express **15**, 7610 (2007).
10. F. Horst, W. M. Green, S. Assefa, S. M. Shank, Y. A. Vlasov, and B. J. Offrein, Opt. express **21**, 11652 (2013).
11. X. Wang, W. Shi, R. Vafaei, N. A. Jaeger, and L. Chrostowski, IEEE Photonics Technol. Lett. **23**, 290 (2011).
12. A. Dhakal, A. Z. Subramanian, P. Wuytens, F. Peyskens, N. Le Thomas, and R. Baets, Opt. letters **39**, 4025 (2014).
13. P. Pintus, F. Di Pasquale, and J. E. Bowers, Opt. express **21**, 5041 (2013).
14. M. Qiu, M. Mulot, M. Swillo, S. Anand, B. Jaskorzynska, A. Karlsson, M. Kamp, and A. Forchel, Appl. Phys. Lett. **83**, 5121 (2003).
15. D. Tan, K. Ikeda, and Y. Fainman, Appl. Phys. Lett. **95**, 141109 (2009).
16. D. T. H. Tan, K. Ikeda, S. Zamek, A. Mizrahi, M. Nezhad, A. Krishnamoorthy, K. Raj, J. Cunningham, X. Zheng, I. Shubin *et al.*, Opt. express **19**, 2401 (2011).
17. W. Shi, X. Wang, W. Zhang, L. Chrostowski, and N. Jaeger, Opt. letters **36**, 3999 (2011).
18. S. K. Selvaraja, P. Jaenen, W. Bogaerts, D. Van Thourhout, P. Dumon, and R. Baets, J. Light. Technol. **27**, 4076 (2009).
19. R. H. French and H. V. Tran, Annu. Rev. Mater. Res. **39** (2009).
20. P. Yeh and H. Taylor, Appl. optics **19**, 2848 (1980).
21. J. Wang, I. Glesk, and L. Chen, Electron. Lett. **51**, 712 (2015).
22. D. Pérez-Galacho, C. Alonso-Ramos, F. Mazeas, X. Le Roux, D. Oser, W. Zhang, D. Marris-Morini, L. Labonté, S. Tanzilli, E. Cassan *et al.*, Opt. letters **42**, 1468 (2017).
23. D. Oser, F. Mazeas, X. L. Roux, D. Pérez-Galacho, O. Alibart, S. Tanzilli, L. Labonté, D. Marris-Morini, L. Vivien, E. Cassan *et al.*, arXiv preprint arXiv:1806.08833 (2018).

FULL REFERENCES

1. A. Rahim, E. Ryckeboer, A. Z. Subramanian, S. Clemmen, B. Kuyken, A. Dhakal, A. Raza, A. Hermans, M. Muneeb, S. Dhoore *et al.*, "Expanding the silicon photonics portfolio with silicon nitride photonic integrated circuits," J. Light. Technol. **35**, 639–649 (2017).
2. A. Z. Subramanian, S. Selvaraja, P. Verheyen, A. Dhakal, K. Komorowska, and R. Baets, "Near-infrared grating couplers for silicon nitride photonic wires," IEEE Photonics Technol. Lett. **24**, 1700–1703 (2012).
3. X. Sun, M. Alam, J. Aitchison, and M. Mojahedi, "Compact and broadband polarization beam splitter based on a silicon nitride augmented low-index guiding structure," Opt. letters **41**, 163–166 (2016).
4. D. Dai, Z. Wang, J. F. Bauters, M.-C. Tien, M. J. Heck, D. J. Blumenthal, and J. E. Bowers, "Low-loss si 3 n 4 arrayed-waveguide grating (de) multiplexer using nano-core optical waveguides," Opt. express **19**, 14130–14136 (2011).
5. E. Ryckeboer, X. Nie, A. Z. Subramanian, D. Martens, P. Bienstman, S. Clemmen, S. Severi, R. Jansen, G. Roelkens, and R. Baets, "Cmos-compatible silicon nitride spectrometers for lab-on-a-chip spectral sensing," **9891**, 98911K (2016).
6. Y. Zuta, I. Goykhman, B. Desiatov, and U. Levy, "On-chip switching of a silicon nitride micro-ring resonator based on digital microfluidics platform," Opt. Express **18**, 24762–24769 (2010).
7. S. Ramelow, A. Farsi, S. Clemmen, D. Orquiza, K. Luke, M. Lipson, and A. L. Gaeta, "Silicon-nitride platform for narrowband entangled photon generation," arXiv preprint arXiv:1508.04358 (2015).
8. W. Xie, T. Stöferle, G. Raino, T. Aubert, S. Bisschop, Y. Zhu, R. F. Mahrt, P. Geiregat, E. Brainis, Z. Hens *et al.*, "On-chip integrated quantum-dot–silicon-nitride microdisk lasers," Adv. Mater. **29**, 1604866 (2017).
9. K. De Vos, I. Bartolozzi, E. Schacht, P. Bienstman, and R. Baets, "Silicon-on-insulator microring resonator for sensitive and label-free biosensing," Opt. express **15**, 7610–7615 (2007).
10. F. Horst, W. M. Green, S. Assefa, S. M. Shank, Y. A. Vlasov, and B. J. Offrein, "Cascaded mach-zehnder wavelength filters in silicon photonics for low loss and flat pass-band wdm (de-) multiplexing," Opt. express **21**, 11652–11658 (2013).
11. X. Wang, W. Shi, R. Vafaei, N. A. Jaeger, and L. Chrostowski, "Uniform and sampled bragg gratings in soi strip waveguides with sidewall corrugations," IEEE Photonics Technol. Lett. **23**, 290–292 (2011).
12. A. Dhakal, A. Z. Subramanian, P. Wuytens, F. Peyskens, N. Le Thomas, and R. Baets, "Evanescent excitation and collection of spontaneous raman spectra using silicon nitride nanophotonic waveguides," Opt. letters **39**, 4025–4028 (2014).
13. P. Pintus, F. Di Pasquale, and J. E. Bowers, "Integrated te and tm optical circulators on ultra-low-loss silicon nitride platform," Opt. express **21**, 5041–5052 (2013).
14. M. Qiu, M. Mulot, M. Swillo, S. Anand, B. Jaskorzynska, A. Karlsson, M. Kamp, and A. Forchel, "Photonic crystal optical filter based on contra-directional waveguide coupling," Appl. Phys. Lett. **83**, 5121–5123 (2003).
15. D. Tan, K. Ikeda, and Y. Fainman, "Coupled chirped vertical gratings for on-chip group velocity dispersion engineering," Appl. Phys. Lett. **95**, 141109 (2009).
16. D. T. H. Tan, K. Ikeda, S. Zamek, A. Mizrahi, M. Nezhad, A. Krishnamoorthy, K. Raj, J. Cunningham, X. Zheng, I. Shubin *et al.*, "Wide bandwidth, low loss 1 by 4 wavelength division multiplexer on silicon for optical interconnects," Opt. express **19**, 2401–2409 (2011).
17. W. Shi, X. Wang, W. Zhang, L. Chrostowski, and N. Jaeger, "Contradirectional couplers in silicon-on-insulator rib waveguides," Opt. letters **36**, 3999–4001 (2011).
18. S. K. Selvaraja, P. Jaenen, W. Bogaerts, D. Van Thourhout, P. Dumon, and R. Baets, "Fabrication of photonic wire and crystal circuits in silicon-on-insulator using 193-nm optical lithography," J. Light. Technol. **27**, 4076–4083 (2009).
19. R. H. French and H. V. Tran, "Immersion lithography: photomask and wafer-level materials," Annu. Rev. Mater. Res. **39** (2009).
20. P. Yeh and H. Taylor, "Contradirectional frequency-selective couplers for guided-wave optics," Appl. optics **19**, 2848–2855 (1980).
21. J. Wang, I. Glesk, and L. Chen, "Subwavelength grating bragg grating filters in silicon-on-insulator," Electron. Lett. **51**, 712–714 (2015).
22. D. Pérez-Galacho, C. Alonso-Ramos, F. Mazeas, X. Le Roux, D. Oser, W. Zhang, D. Marris-Morini, L. Labonté, S. Tanzilli, E. Cassan *et al.*, "Optical pump-rejection filter based on silicon sub-wavelength engineered photonic structures," Opt. letters **42**, 1468–1471 (2017).
23. D. Oser, F. Mazeas, X. L. Roux, D. Pérez-Galacho, O. Alibart, S. Tanzilli, L. Labonté, D. Marris-Morini, L. Vivien, E. Cassan *et al.*, "Coherency-broken bragg filters: surpassing on-chip rejection limitations," arXiv preprint arXiv:1806.08833 (2018).